Dual-Active-Center of Polyimide and Triazine Modified Atomic-Layer Covalent Organic Frameworks for High-Performance Li Storage

Genfu Zhao, Huani Li, Zhihui Gao, Lufu Xu, Zhiyuan Mei, Sheng Cai, Tingting Liu, Xiaofei Yang, Hong Guo,* and Xueliang Sun*

Covalent organic frameworks (COFs) have received great attention as electrode materials in the lithium-ion batteries due to their exceptional crystallinity, easily chemical modification, and adjustable porous distribution. However, their practical application remains hindered by the insufficient Li$^+$ active sites and long ion diffusion in the bulk materials. To tackle those issues, combining the virtues of high stable skeleton structure of large molecular, atomic-layer thickness feature, and multi-active sites, a novel atomic-layer COF cathode (denoted as E-TP-COF) with a dual-active-center of C=O and C=N group is developed. The atomic-layer thick structure improves the capturing and diffusion of Li-ion. Both active sites of C=N and C=O groups generate more capacity. The large molecular structure avoids the dissolubility challenge in electrolytes. As a result, the lithium-ion batteries assembled with E-TP-COF delivers a high initial capacity of 110 mAh g^{-1} with a high capacity retention of 87.3% after 500 cycles. Furthermore, the Li$^+$ diffusion mechanism is also confirmed through in(ex) situ technology and density functional theory calculation in detailing. This new strategy may exploit an important application of COFs in electrochemical energy storage and conversion.

1. Introduction

Lithium-ion batteries (LIBs) play an irreplaceable role in our life and have been widely applied in portable electronics and electric vehicles.[1–3] With the increasingly demand, the limited Li resource on the earth will be fleetly consumed, which goes against the sustainable development. It is urgently required to develop high-efficiency Li storage materials. Compared with

inorganic electrodes,[4–8] organic materials possess environmental-friendliness, cost-effectiveness, easy functionalization, and renewability, and thus have attracted widespread interests.[9–11] However, intrinsic shortcomings (including poor conductivity, limited active sites, and dissolution in electrolyte) hinder their further application.[12] Therefore, constructed unique organics introducing conductive carbon matrix or insertion reversible multi-electron redox centers to the organic porous and periodic framework materials could improve fast Li$^+$/e$^-$ transport, and are beneficial for the enhanced reversible capacities and cyclic stability of assembled LIBs.[13,14]

Covalent organic frameworks (COFs), as this interesting kind of organics, have plentifully excellent features, such as high surface area and crystallinity, easily chemical modification, and adjustable pore distribution.[15–18] Simultaneously, COFs belonging to large molecular structures show prominent stability than organic small molecules, and are not easily dissolved in solvents. Therefore, they are broadly involved into the catalysis, separation, and energy storage fields.[19–24] However, the traditional 2D COFs are still suffering from stacking into bulk materials via π–π interaction. The Li$^+$ transport distance is prolonged and some active sites are blocked in bulk COFs. Meanwhile, most of current reported COF electrodes only contain a single activity redox group due to the limit of synthesized methods, which inevitably leads to low theoretical capacity and practical capacity output.[25–29] Moreover, large amount of carbon materials such as nanotube and rGO are normally introduced in those works to improve their performance, generating practically low capacity and utilization.[30–34] These factors seriously hinder the further improvement of electrochemical performance of the assembled LIBs.

To solve these bottlenecks, designing multi-activity COFs can increase its capacity output effectively. For example, Zhang et al. and our previous works exhibit enhanced electrochemical performance for the anode.[29,32] However, there are few reports on dual-active-site cathode, because the strategy for anode is difficult to be realized in cathode during the synthetic process, which is involved metal-ion introduction. At the same time, exfoliating the bulk COFs into few-layer or nano-sheet COFs is proved as another

Dr. G. Zhao, H. Li, Z. Gao, L. Xu, Z. Mei, S. Cai, T. Liu, Prof. H. Guo
School of Materials and Energy
Yunnan Key Laboratory for Micro/Nano Materials and Technology
Yunnan University
No. 2, Green Lake North Road, Kunming 650091, China
E-mail: guohong@ynu.edu.cn
X. Yang, Prof. X. Sun
Nanomaterials and Energy Lab Department of Mechanical
and Materials Engineering
Western University
London, ON N6A 5B9, Canada
E-mail: xsun9@uwo.ca

valid measure to promote their improvement of electrochemical performance.[30–34] In fact, taking only one measure could enhance its properties very limited. Furthermore, the low electrical conductivity of COFs also should be attention in the practical applications. Therefore, how to construct dual-active-site modified few-layer COFs cathode material is highly desired. As fast as our knowledge, no work has been reported on dual-active-site modified few-layer COF as the cathode material for LIBs.

Herein, we report a dual-active-center of C=O on polyimide and C=N on triazine modified atomic-layer COF (E-TP-COF) using mechanical exfoliation way. The bulk COF (TP-COF) is obtained by condensing active site materials of 1,3,5-tris-(4-aminophenyl)triazine (Ta)[35] and pyromellitic dianhydride (Pm)[36] in the mixed solution of *N*-methyl pyrrolidone (NMP), isoquinoline, and mesitylene (**Figure 1**a–f). Then, the bulk TP-COF is exfoliated using ball-milling method and the obtained few-layered E-TP-COF possesses a thickness of around 2.6 nm, equaling to 14 atomic layers (Figure 1g). The dual-active-center regulated few-layered E-TP-COF is, for the first time, introduced as the cathode material into the LIBs. The large molecular structure of this unique E-TP-COFs can avoid the dissolubility challenge in electrolytes, and thus enhance the stability obviously during the cycling than the small molecular organic cathode reported recently. Both active sites of C=N and C=O groups generate more capacity than the current COFs cathode with single active functional site. Moreover, atomic-layer thick

structure is more fit for the capturing and diffusion of Li-ion, leading to enhanced dynamic performance of the battery system. Therefore, we expect this study can create a novel technology for developing highly-effective LIBs and accelerate the application of COFs in energy storage and conversion fields.

2. Results and Discussions

TP-COF was synthesized via a solvothermal method with starting materials of Ta and Pm (Scheme S1, Supporting Information).[37–39] Figure S1a, Supporting Information displays the Fourier transform infrared (FT-IR) spectrometry of Ta, Pm, and TP-COF. As can be seen, two characteristic peaks at 1776 and 1725 cm^{-1} in the spectrum of TP-COF, belong to the asymmetric and symmetric vibrations of C=O group on imide rings.[37] The C=O group comes from Pm, while the imide rings is generated from chemical reaction between −NH$_2$ on Ta and acid anhydride on Pm. The peak at 1360 cm^{-1} is ascribed to the C−N−C.[31] The successful synthesis of TP-COF is further consolidated by the disappeared −NH$_2$ group, indicating the complete covalence between Ta and Pm. The crystallinity of TP-COF is studied by the powder X-ray diffraction (PXRD). Figure 1b shows the PXRD patterns of experimental result, simulated AB stacking, AA stacking, and the Pawley refinement. As can be seen, the experimental pattern displays several peaks at 2θ = 2.81°, 5.05°, 5.85°, 7.75°, 10.31°,
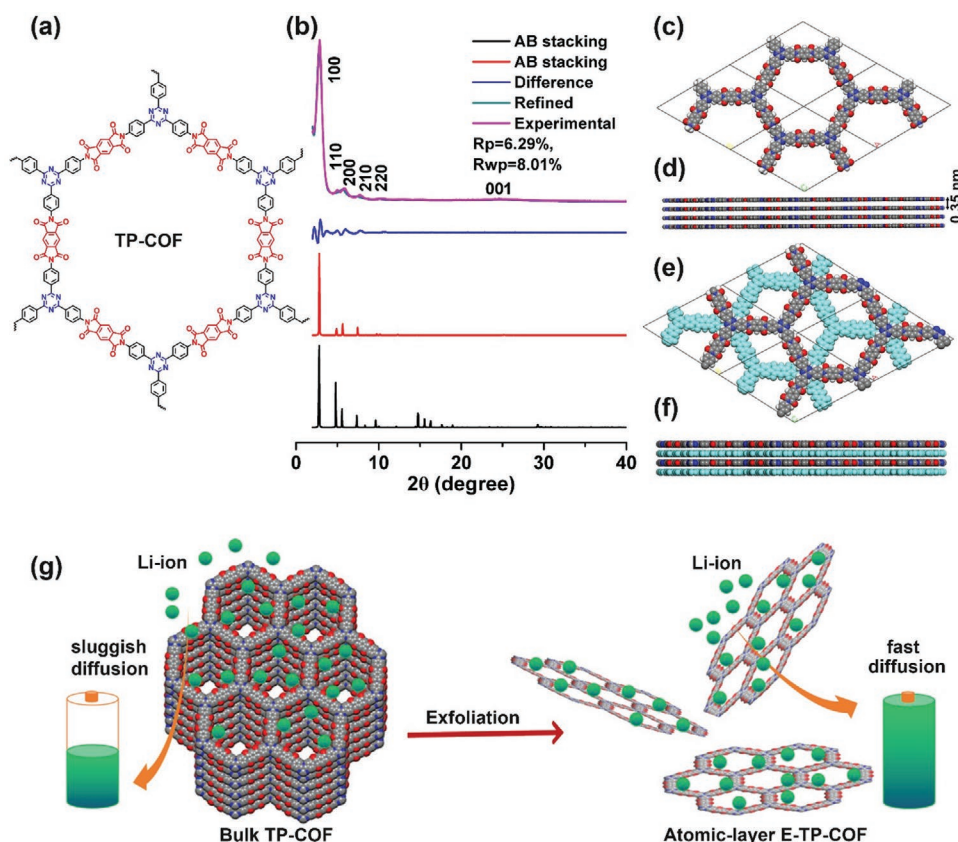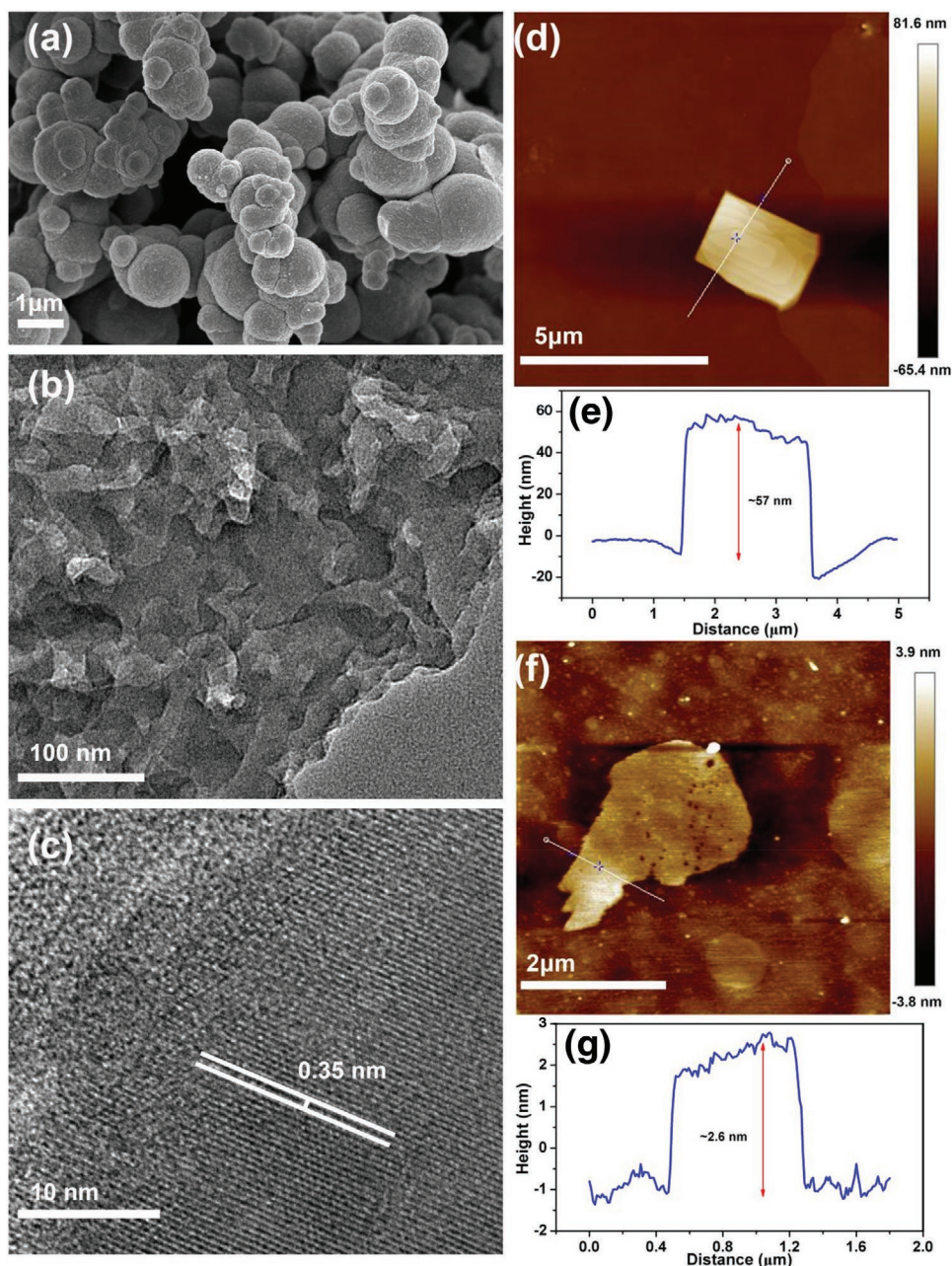

Figure 1. a) Chemical structure of dual-active-center modified TP-COF; b) PXRD patterns of TP-COF with experimental, Pawley refined, difference, AA stacking, and AB stacking; calculated models for c,d) AA-stacking and for e,f)AB-stacking; g) the schematic representation of exfoliated process for TP-COF into E-TP-COF as cathodes for Li-ion battery.

and 25.6°, corresponding to the (100), (110), (200), (210), (220), and (001) planes of TP-COF,[39] which matches well with the simulated pattern of AA stacking (Figure 1c–f). Additionally, the refinement results in Figure 1b and Table S3, Supporting Information further consolidates the successful synthesis of TP-COF with high crystallinity. The C atom of imide ring is certified by the solid-state ^{13}C magic angle spinning NMR. As exhibited in Figure S1b, Supporting Information, the peak at ≈164 ppm can be assigned to the carbonyl carbon of the imide ring. Other overlapping peaks are well ascribed to the C species in benzene ring. At same time, no distinct peaks at chemical shift ≈177 ppm of starting materials can be found, implying the imide ring-closing interaction is thorough. The pore distribution of TP-COF is evaluated by Brunauer–Emmett–Teller (BET) measurements. Figure S1c, Supporting Information exhibits the Nitrogen (N_2) sorption–desorption and implies the reversible type IV isotherms with a slight hysteresis in the process of desorption. Therefore, the BET surface area is calculated to be 960 m^2 g^{-1} based on the N_2 sorption–desorption. In addition, the pore diameter distribution of TP-COF is obtained from the non-local density functional theory (DFT), suggesting mesopores feature of ≈3.2 nm (Figure S1d, Supporting Information) that is close to the theoretical values of 3.3 nm (Scheme S1, Supporting Information). The small difference of pore size between experimental result and theoretical simulation might be assigned to the serrated stacking with adjacent sheets slipped. X-ray photoelectron spectroscopy (XPS) is carried out to determinate the surface element of TP-COF. The XPS survey spectrum (Figure S2a, Supporting Information) shows the C, N, and O elements. Furthermore, the high resolution XPS spectra of C 1s (Figure S2b, Supporting Information), N 1s (Figure S2c, Supporting Information), and O 1s (Figure S2d, Supporting Information) can further certify the structure of synthesized TP-COF. Consequently, above-mentioned results confirm that high crystalline TP-COF is successfully prepared.

The atomic-layer E-TP-COF is obtained by exfoliation the bulk TP-COF. The structural stability of original TP-COF against solvents is first investigated by immersing TP-COF in various solvents (organic solvents, acid) and then made to stand for 4 days. The optical images in Figure S3a, Supporting Information show that TP-COF has negligible color change or dissolution in the solvents. The structural stability is further confirmed by the unchanged FT-IR spectra in Figure S3b, Supporting Information and PXRD patterns in Figure S3c, Supporting Information. The structure of TP-COF is not stable under the strong basic solvent. This is because the imide ring on the TP-COF is decomposed under the strong basic solvents. The high stability of TP-COF against the solvents provides opportunities to develop stable and safe batteries. It is well known that the electrochemical performance of electrode materials is highly dependent on the exposed active sites and ion transport capability. In the bulk TP-COF, its utilization in the batteries will be hindered by the limited active sites and poor ion transport because of long transport distance. With this in mind, the bulk TP-COF is further exfoliated into few-layered nano-sheet via a ball-milling method. These exfoliation products are further checked by scanning electron microscopy (SEM), transmission electron microscopy (TEM), and atomic force microscopy (AFM). As displayed in **Figure 2**a, the bulk TP-COF presents a sphere-like morphology with a diameter of roughly 1 μm. After exfoliation, the sphere-like TP-COF

is completely transferred into nano-sheet-type E-TP-COF (Figure S4a, Supporting Information), implying the successful exfoliation process. Second, the sphere-like structure of TP-COF is observed in TEM image (Figure 2b) with aggregation of plentiful petals. More importantly, the high resolution TEM image (Figure 2c) presents the apparent interplanar distance of 0.35 nm, which is in highly accordance with the theoretical values of 0.35 (Figure 1d), implies outstanding crystalline of TP-COF. For the E-TP-COF, the few-layer nano-sheet is overtly found in TEM image (Figure S5, Supporting Information), and the interplanar distance disappears from the high resolution TEM image (Figure S5, Supporting Information), certifying continuous mechanical exfoliation. Thicknesses of COFs are measured by AFM analysis. Before the exfoliation, the TP-COF shows larger thickness with ≈60 nm (Figure 2d,e). However, the E-TP-COF has ultrathin thickness with ≈2.6 nm (Figure 2f,g). Considering the interplanar distance of 0.35 nm between adjacent layers, we can conclude that the E-TP-COF is consisted by ≈14 atomic layers.[30] These results can give a powerful evidence that E-TP-COF has been successfully exfoliated into ultrathin 2D few-layer. The EDS mapping (Figure S4c–f, Supporting Information) suggests the uniform distribution of C, N, and O elements on the surface of E-TP-COF. For studying the structure integrity of E-TP-COF, the FT-IR spectrum, and PXRD of pristine TP-COF and exfoliated E-TP-COF are measured. Similar profiles of TP-COF and E-TP-COF in the FT-IR spectrum (Figure S6a, Supporting Information) illustrates the same chemical structure. And the PXRD pattern of E-TP-COF (Figure S6b, Supporting Information) still has the (100) planes at 2.8°, reveals that E-TP-COF maintains the ordered and periodic framework after exfoliation. In thermo-gravimetric curves, both TP-COF and E-TP-COF show negligible weight loss before 500 °C, suggesting high thermal stability (Figure S6c, Supporting Information). According the aforementioned analysis, it can conclude that the TP-COF is successfully exfoliated into E-TP-COF and the structure is well-maintained during the exfoliated process.

The electrochemical performance of bulk TP-COF and sheet-type E-TP-COF as cathode materials in LIBs are studied by cyclic voltammogram (CV). As displayed in **Figure 3**a (blue curve), both TP-COF and E-TP-COF present three couples of reduction/oxidization peaks at 1.85/2.16 V, 2.25/2.44 V and 2.25/2.86 V (vs Li$^+$/Li), ascribing to the reversible lithiation/delithiation procedures of C=O and C=N groups. The reduction potential of C=N overlaps with the C=O at ≈2.25 V, corresponding the Li-ion insertion into C=N group in triazine, and the oxidation peak at 2.85 V is ascribed to the C=O. Due to the existence of dual-site C=O and C=N, the continuous procedures of reduction/oxidization lead to unobvious and indiscernible redox potential.[25,27,31,36] It is noteworthy to mention that the peak current of E-TP-COF is much higher than its counterpart, which can be attributed to the more exposed and higher utilizated active sites of C=O and C=N. And the Li-ion can rapidly diffuse in the E-TP-COF than TP-COF. During cycling testing, the CV curves are almost overlapped, indicating high reversibility and cycling stability of E-TP-COF electrode (Figure S7, Supporting Information). The difference in electrochemical performance of TP-COF and E-TP-COF electrode is further investigated by galvanostatic charging–discharging process at a current density of 200 mA g^{-1}. As displayed in Figure 3b, for the E-TP-COF electrode, two discharge plateaus at 2.25 and 1.85 V are observed, attributing to the lithiation processes of

**ADVANCED
SCIENCE NEWS**

www.advancedsciencenews.com

**ADVANCED
FUNCTIONAL
MATERIALS**

www.afm-journal.de

Figure 2. a) SEM image of TP-COF; b) TEM image of TP-COF; c) HRTEM image of TP-COF; AFM images of d) TP-COF and f) E-TP-COF; the measured thickness of e) TP-COF and g) E-TP-COF.

C=O and C=N groups, which is coincided well with CV results. The continuous procedures of reduction/oxidization of dual-site C=O and C=N generate to unobvious and indiscernible redox potential and discharge and charge plateau. The capacity utilization efficiency for E-TP-COF is 42.9% of its theoretical capacity (256 mA g^{-1}, calculated according to two-electron redox reaction per imide and three-electron triazine units, Scheme S3, Supporting Information). Attentively, taking into account of one electron (or two electrons) is involved in each triazine unit, the theoretical capacity will be calculated to be ≈ 171 (for one electron) and 213 mAh g^{-1} (for two electron), respectively. Therefore, for the sufficiency of the utilization of triazine center, the three electrons are

adopted as the theoretical capacity and theoretical computational model, which leads to low utilization of theoretical capacity. However, the E-TP-COF shows high specific capacity with 110 mAh g^{-1} than TP-COF with 25 mAh g^{-1}, implying obviously enhanced utilization of active-site during the exfoliated procedure. For the bare E-TP-COF cathode, this high specific capacity nearly exceeds other COFs with adding carbon materials (Table S3, Supporting Information), which further highlights the preponderance of dual-active-site regulated atomic-layer COF.

The underlying mechanism for the huge difference in capacity output is further clarified by Li-ion diffusion kinetics study using electrochemical impedance spectroscopy (EIS).
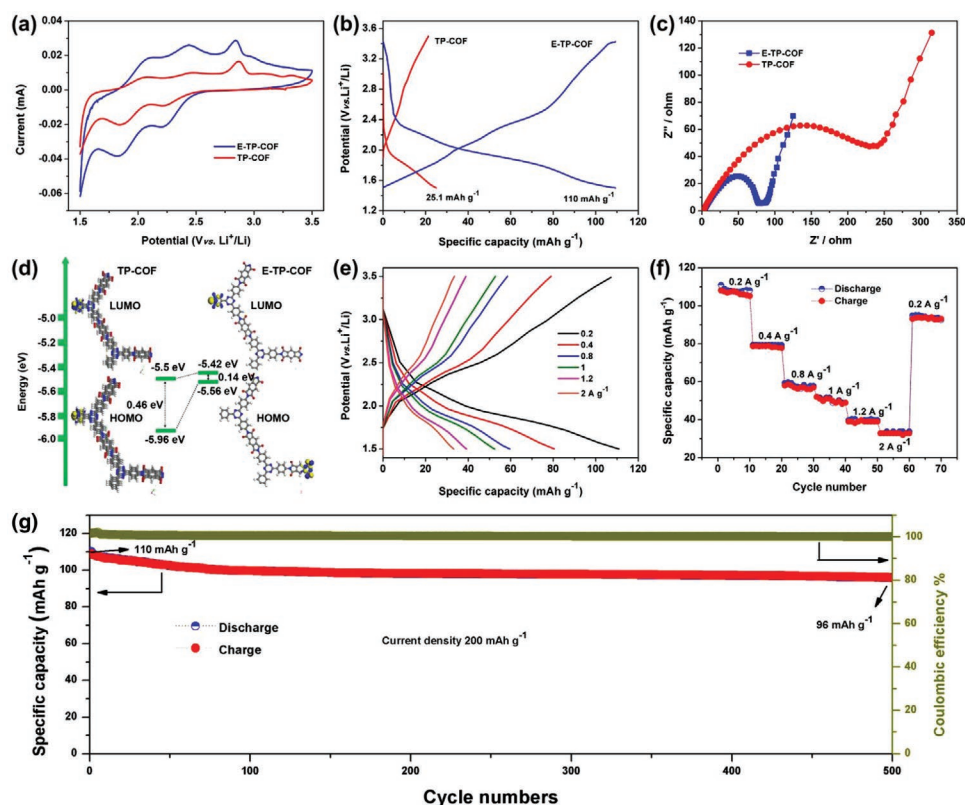
Figure 3. a) CV curves of E-TP-COF and TP-COF at 0.1 mV s^{-1}; b) galvanostatic charge–discharge curves of E-TP-COF and TP-COF at 0.2 A g^{-1}; c) Nyquist plots of E-TP-COF and TP-COF; d) calculated HOMO and LUMO value of E-TP-COF and TP-COF based on the DFT calculation; e) charge–discharge curves at various current rates and f) rate performance for E-TP-COF electrode; g) long-term cycling stability of E-TP-COF at 0.2 A g^{-1}.

The EIS curves of the two electrodes present a semi-circle at high frequency and a sloping line at low frequency, assigning to the charge-transfer resistance (R_{ct}) and Warburg impedance. The R_{ct} is derived from the reaction kinetics, while the Warburg impedance is related to the ion transport.[31] The reduced R_{ct} value from bulk TP-COF to exfoliated E-TP-COF indicates that the charge transfer behavior in E-TP-COF electrode is more superior to TP-COF electrode. This exfoliated technique improves the overall electrochemical performances (Figure 3c). To understand the mechanism at the molecular level, the values of highest-occupied/lowest-unoccupied molecular orbital (HOMO or LUMO) for TP-COF and E-TP-COF are studied, respectively. The energies distribution of the HOMO and LUMO orbitals for TP-COF and E-TP-COF are provided in Figure 3d. The band gap between HOMO (−5.5 eV) and LUMO (−5.96 eV) orbitals for TP-COF is determined to be 0.46 eV, which is 0.14 eV higher compared with that of E-TP-COF (HOMO: −5.42 eV, LUMO: −5.56 eV). The narrow band gap of E-TO-COF means lower energy barrier for metal-ion or electron transport, thus better rate performance and higher discharge capacity are expected.

Figure 3e,f exhibit the rate performance of E-TP-COF electrode evaluated at various current densities from 0.2 to 2 A g^{-1}. As can be seen, the E-TP-COF electrode delivers a highly initial capacity of over 110 mAh g^{-1} at 0.2 A g^{-1} and maintains a capacity of over 30 mAh g^{-1} at 2 A g^{-1}. The related values are much higher than its counterpart of TP-COF (25 mAh g^{-1} at

0.2 A g^{-1} and 0.3 mAh g^{-1} at 2 A g^{-1}) (Figure S8, Supporting Information). The higher capacity output and better rate performance of E-TP-COF electrode are coincided well with the TEM, CV, EIS, and HOMO–LUMO calculation results that the more available active sites, reduced ion transport distance, low energy barrier of ion, and electron transport improves the electrochemical reaction kinetics. Additionally, it should be mentioned that a reversible capacity of 96 mAh g^{-1} can be recovered when the current density is returned to 0.2 A g^{-1}, which indicates that excellent structural stability of E-TP-COF under high current density operation, which is of significance to realize long cycling life of the assembled LIBs. The cycling stability of E-TP-COF electrode under a current density of 0.2 A g^{-1} is shown in Figure 3g. The E-TP-COF electrode reflects excellent cycling stability within a high capacity retention of roughly 87.3% (96 mAh g^{-1}) after 500 cycles. The cycling stability is superior to the electrochemical performance of recently reported triazine and pyromellitic dianhydride-based COFs (Table S1, Supporting Information). In contrast, only a low capacity of 5 mAh g^{-1} is retained for the TP-COF electrode (Figure S9, Supporting Information), implying the poor stability and insufficient reactive center utilization of TP-COF electrode. The results above consolidate that the dual-active-center modified atomic-layer COFs are promising candidates as cathode materials for LIBs.

Considering the capacity output is highly dependent on the utilization of active groups, thus the Li lithiation/delithiation process is evaluated by FR-IR and XPS. The C=O and C=N
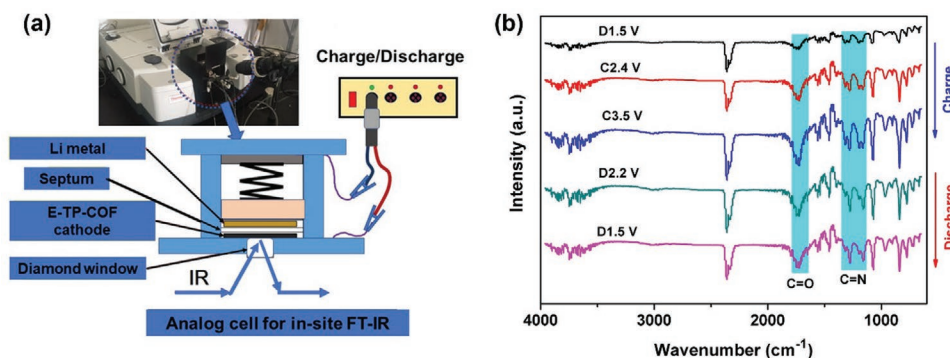
Figure 4. a) The in situ FT-IR spectrum equipment pattern and b) spectral changes of the E-TP-COF electrode at different discharge and charge states.

groups can store one Li$^+$ to form C—O—Li and C—N—Li species, respectively. The electronegativity of C=O center is stronger than C=N, resulting in the Li-ion first interact with C=O. In addition, the C=O in pyromellitic dianhydride receives two Li-ions, due to reduction of reactivity of C=O group (Scheme S4, Supporting Information). The C=N in triazine can receive three Li-ions (Scheme S4, Supporting Information). Therefore, one unit of E-TP-COF can interact with 30 Li-ions in total during the discharged/charged processes (Scheme S4, Supporting Information). This reversible reaction procedure between E-TP-COF and Li-ion is deduced using diverse in site techniques during the charged/discharged procedures at various potential (**Figure 4**a). During the discharging process

(D2.2 and D1.5 V), the intensity of the peaks at 1776, 1725, and 1508 cm^{-1}, ascribing to the C=O and C=N in triazine ring vibration gradually decrease (Figure 4b), owing to the consumption of these active sites by Li-ions. In the following charging process (C2.4 and C3.5 V), the intensity those peaks obviously increase. It can be attributed to the recovery of active sites and demonstrates high revisability of active sites in E-TP-COF, which provides an evidence to explain the good cycling stability in LIBs. Moreover, the delithiation/lithiation processes are further certified by XPS spectra analysis. As shown in **Figure 5**a, in spectrum of N 1s, two major peaks located at 401.4 and 398.5 eV are observed and they are assigned to the C—N and faint C=N, respectively. After the charging at potential 2.4 to 3.5 V for the
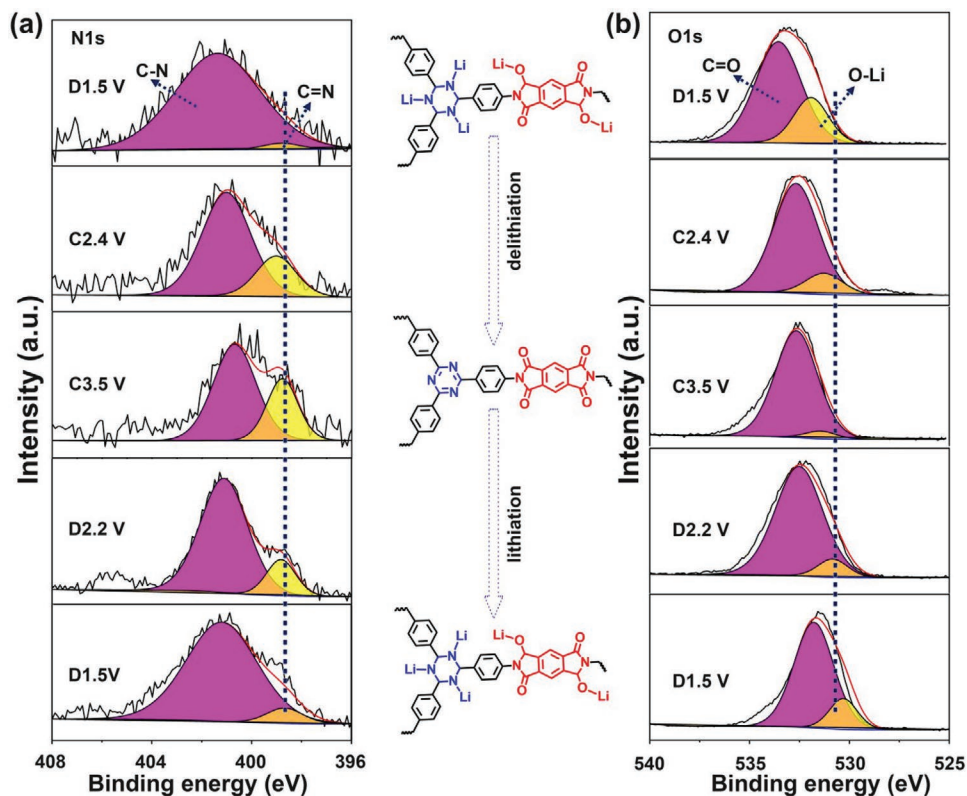
Figure 5. a) Comparison of XPS spectra of N 1s for E-TP-COF electrode discharged at 1.5 V, charged to 2.4 and 3.5 V, and charged to 2.2 and 1.5 V; b) comparison of XPS spectra of O 1s for E-TP-COF electrode discharged at 1.5 V, charged to 2.4 and 3.5 V, and charged to 2.2 and 1.5 V.
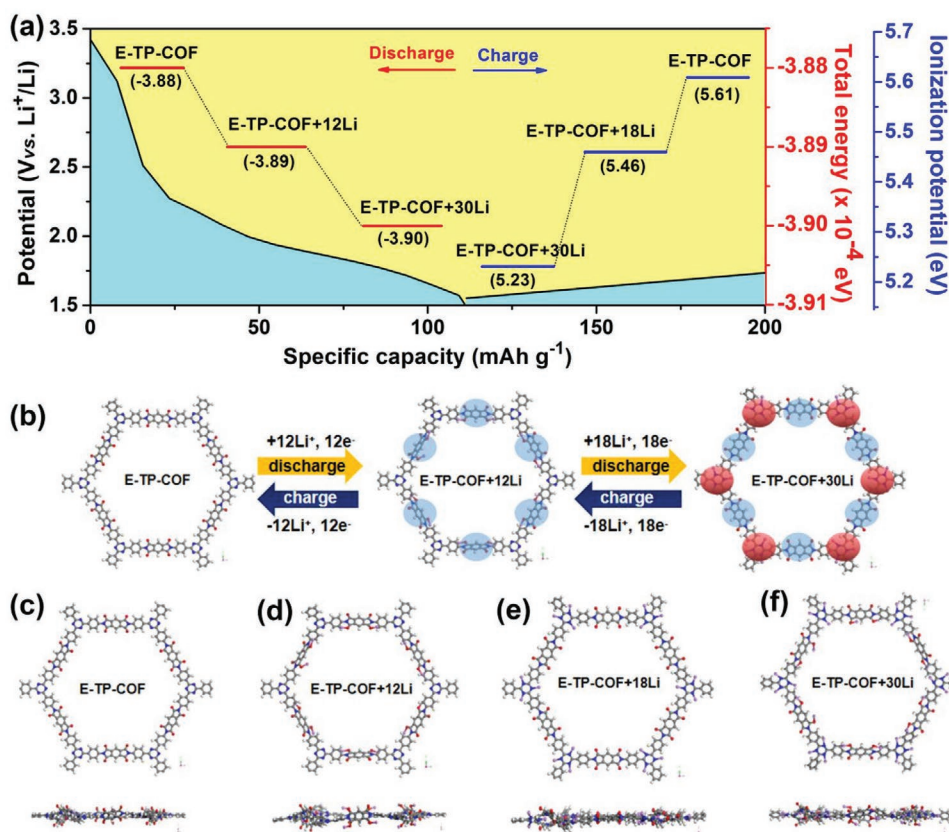
Figure 6. a) Proposed lithiation pathway for the E-TP-COF electrode. The left axis shows the redox potential versus Li⁺/Li, and the right axis shows the total energy and ionization potential of various lithiated E-TP-COF structures. b) Structural evolution during the lithiation/delithiation procedure atomic colors: white: H, gray: C, red: O, and blue: N). The binding sites between Li and the C=O and C=N groups are indicated by blue and red spheres, respectively. Schematics of the optimized structures at different stages of c) Li of E-TP-COF, d) E-TP-COF+12Li, e) E-TP-COF+18Li, and f) E-TP-COF+30Li, respectively.

delithiation process, the peak of C=N obviously enhances, demonstrating the C=N group reversion from the C—N—Li species. However, after again discharging to 1.5 V, the C=N peak is once expanded, suggesting excellently reversible reaction of few-layer E-TP-COF with Li-ion. Furthermore, the similar changes of XPS spectrum for O 1s can be found. As shown in Figure 5b, for the discharged electrode E-TP-COF, the XPS spectrum of O 1s displays two major peaks, corresponding to the C=O and O—Li bonds in E-TP-COF framework. The peaks undergo the weakening and rebounding during the charged/discharged procedures, which can further prove the reversible reaction for Li storage in the dual-active-center modified few-layer E-TP-COF.[40,41] Above analysis demonstrates the preeminently reversible and high-performance Li storage behaviors of E-TP-COF material.

To deeply understand the multiple lithiation process of dual-active-center modified few-layer E-TP-COF electrode material, the DFT calculation is used for simulating the electrochemical Li storage process.[42,43] In principle, the E-TP-COF can receive 12 Li-ions (denoted as E-TP-COF+12Li) at the C=O sites and 18 Li-ions (denoted as E-TP-COF+18Li) at the C=N sites. Totally, 30 Li-ions can be stored by E-TP-COF (denoted as E-TP-COF+30Li) based on the dual-active-center concept. The total energy for fresh E-TP-COF electrode is calculated

to be -3.88×10^{-4} eV. During lithiation, the energies of E-TP-COF+12Li and E-TP-COF+30Li are reduced to -3.89×10^{-4} and -3.9×10^{-4} eV, respectively (**Figure 6**a). Therefore, the difference value of total energy between as-made E-TP-COF and E-TP-COF+12Li is calculated to be -0.01×10^{-4} eV. With same analysis, the difference value between E-TP-COF and E-TP-COF+30Li is -0.02×10^{-4} eV. The difference value of total energy for E-TP-COF to E-TP-COF+12Li is obvious smaller than the E-TP-COF to E-TP-COF+30Li, implying the Li-ion preferentially interact with the active site of C=O group. However, during the charged procedure, the ionization potentials of E-TP-COF+30Li, E-TP-COF+18Li, and E-TP-COF are calculated to be 5.23, 5.46, and 5.61 eV, respectively (Figure 6a). The lower ionization potential indicates more easier to loss the Li-ion. Therefore, the E-TP-COF+30Li easily losses 12 Li-ions to return the E-TP-COF+18Li state, and the E-TP-COF+18Li sequentially losses the 18 Li-ions to return back to the initial state. The discharging/charging processes are further derived in the Figure 6b. And the Figure 6c–f shows the optimized structures various state, respectively. In addition, we assess the different energy on the various states with electronic energy, core-core repulsion, total energy, ionization potential, and heat of formation for each optimized structure. From the Table S2, Supporting Information, we can find that the electronic energy in

E-TP-COF+12Li is most low than other states of E-TP-COF+18Li and E-TP-COF+30Li. Further, the surface electrostatic potentials for E-TP-COF, E-TP-COF+12Li, E-TP-COF+18Li, and E-TP-COF+30Li are described in Figure S10, Supporting Information. Moreover, Figure S11, Supporting Information exhibits the EIS plots of E-TP-COF electrode before and after cycling (100 cycles). It shows that the R_{ct} decreases from 80.3 (before cycling) to the 65.1 Ω (after cycling), indicating fast and stable reaction kinetics of the cathode material.[44–46] Above the electronic energy and surface electrostatic potentials imply that the C=O center primarily obtains the Li-ion than C=N group, and both the sites have excellent and reversible property for Li storage with stable reaction kinetics.

3. Conclusions

In this study, we, for the first time, explored the dual-active-center of C=O and C=N groups modified few-layer COFs and investigated the structure-performance relationship in LIBs. This novel material has excellently structural stability, shorten Li-ion diffusion distance, and low energy barrier, and shows prominently electrochemical performance as the cathode in the LIBs. The high capacity output and long-term stability for the functional E-TP-COF electrode generate from the abundant active center and few-layer structure, which are beneficial for the fast Li-ion diffusion. The electrochemical mechanism for Li storage is evolved in detail by the in situ FT-IR, XPS, and DFT calculation. This strategy might play a crucial role in electrochemical energy storage and conversion, and can be easily broadened other electronic devices as the important material.

4. Experimental Section

The experimental processes are provided in the Supporting Information.
    The chemical reagents, characterization, experimental synthetic procedure of TP-COF and E-TP-COF, electrochemical measurement and others materials are shown in the Supporting Information.

Supporting Information

Supporting Information is available from the Wiley Online Library or from the author.

Conflict of Interest

The authors declare no conflict of interest.

Data Availability Statement

Research data are not shared.

[1] T. Kim, W. Song, D.-Y. Son, L. K. Ono, Y. Qi, *J. Mater. Chem. A* **2019**, *7*, 2942.
[2] P. Li, J.-Y. Hwang, Y.-K. Sun, *ACS Nano* **2019**, *13*, 2624.
[3] Q. Zhao, Y. Lu, J. Chen, *Adv. Energy Mater.* **2017**, *7*, 1601792.
[4] X. R. Han, X. T. Guo, M. J. Xu, H. Pang, Y. W. Ma, *Rare Met.* **2020**, *39*, 1099.
[5] J. T. Hu, J. X. Zheng, F. Pan, *Acta Phys.-Chim. Sin.* **2019**, *35*, 361.
[6] H. Hu, J. Zhang, J. Guan, X. W. Lou, *Angew. Chem., Int. Ed.* **2016**, *55*, 9514.
[7] H. Liu, H. Guo, B. Liu, M. Liang, Z. Lv, K. R. Adair, X. Sun, *Adv. Funct. Mater.* **2018**, *28*, 1707480.
[8] Y. Zhang, B. Liu, T. Borjigin, S. Xia, X. Yang, S. Sun, H. Guo, *J. Power Sources* **2020**, *450*, 227696.
[9] Z. Song, H. Zhou, *Energy Environ. Sci.* **2013**, *6*, 2280.
[10] T. Ma, Q. Zhao, J. Wang, Z. Pan, J. Chen, *Angew. Chem., Int. Ed.* **2016**, *55*, 6428.
[11] T. Sun, Z.-J. Li, H.-G. Wang, D. Bao, F.-L. Meng, X.-B. Zhang, *Angew. Chem.* **2016**, *128*, 10820.
[12] S. Lee, J. Hong, K. Kang, *Adv. Energy Mater.* **2020**, *10*, 2001445.
[13] H. Wu, Q. Meng, Q. Yang, M. Zhang, K. Lu, Z. Wei, *Adv. Mater.* **2015**, *27*, 6504.
[14] S. Muench, A. Wild, C. Friebe, B. Haupler, T. Janoschka, U. S. Schubert, *Chem. Rev.* **2016**, *116*, 9438.
[15] A. P. Cote, A. I. Benin, N. W. Ockwig, M. O'keeffe, A. J. Matzger, O. M. Yaghi, *Science* **2005**, *310*, 1166.
[16] P. J. Waller, F. Gándara, O. M. Yaghi, *Acc. Chem. Res.* **2015**, *48*, 3053.
[17] S. Kandambeth, K. Dey, R. Banerjee, *J. Am. Chem. Soc.* **2019**, *141*, 1807.
[18] Z. Lei, X. Chen, W. Sun, Y. Zhang, Y. Wang, *Adv. Energy Mater.* **2019**, *9*, 1801010.
[19] R. Tao, X. Shen, Y. Hu, K. Kang, Y. Zhang, S. Luo, S. Yang, W. Li, S. Lu, Y. Jin, L. Qiu, W. Zhang, *Small* **2020**, *16*, 1906005.
[20] X. Chen, Y. Li, L. Wang, Y. Xu, A. Nie, Q. Li, F. Wu, W. Sun, X. Zhang, R. Vajtai, P. M. Ajayan, L. Chen, Y. Wang, *Adv. Mater.* **2019**, *31*, 1901640.
[21] M. G. Mohamed, C.-C. Lee, A. F. M. EL-Mahdy, J. Lüder, M.-H. Yu, Z. Li, Z. Zhu, C.-C. Chueh, S.-W. Kuo, *J. Mater. Chem. A* **2020**, *8*, 11448.
[22] S. Yuan, X. Li, J. Zhu, G. Zhang, P. V. Puyveldeb, B. Van der Bruggen, *Chem. Soc. Rev.* **2019**, *48*, 2665.
[23] T. Sun, J. Xie, W. Guo, D.-S. Li, Q. Zhang, *Adv. Energy Mater.* **2020**, *10*, 1904199.
[24] M. G. Mohamed, E. C. Atayde Jr., B. M. Matsagar, J. Na, Y. Yamauchi, K. C.-W. Wu, S.-W. Kuo, *J. Taiwan Inst. Chem. Eng.* **2020**, *112*, 180.
[25] G. Wang, N. Chandrasekhar, B. P. Biswal, D. Becker, S. Paasch, E. Brunner, M. Addicoat, M. Yu, R. Berger, X. Feng, *Adv. Mater.* **2019**, *31*, 1901478.
[26] S. Gu, S. Wu, L. Cao, M. Li, N. Qin, J. Zhu, Z. Wang, Y. Li, Z. Li, J. Chen, Z. Lu, *J. Am. Chem. Soc.* **2019**, *141*, 9623.
[27] E. Vitaku, C. N. Gannett, K. L. Carpenter, L. Shen, H. D. Abruña, W. R. Dichtel, *J. Am. Chem. Soc.* **2020**, *142*, 16.

**ADVANCED
SCIENCE NEWS**

www.advancedsciencenews.com

**ADVANCED
FUNCTIONAL
MATERIALS**

www.afm-journal.de

[28] X. Li, H. Wang, H. Chen, Q. Zheng, Q. Zhang, H. Mao, Y. Liu, S. Cai, B. Sun, C. Dun, M. P. Gordon, H. Zheng, J. A. Reimer, J. J. Urban, J. Ciston, T. Tan, E. M. Chan, J. Zhang, Y. Liu, *Chem* **2020**, *6*, 933.

[29] G. Zhao, Y. Zhang, Z. Gao, H. Li, S. Liu, S. Cai, X. Yang, H. Guo, X. Sun, *ACS Energy Lett.* **2020**, *5*, 1022.

[30] S. Wang, Q. Wang, P. Shao, Y. Han, X. Gao, L. Ma, S. Yuan, X. Ma, J. Zhou, X. Feng, B. Wang, *J. Am. Chem. Soc.* **2017**, *139*, 4258.

[31] Z. Wang, Y. Li, P. Liu, Q. Qi, F. Zhang, G. Lu, X. Zhao, X. Huang, *Nanoscale* **2019**, *11*, 5330.

[32] H. Zhang, W. Sun, X. Chen, Y. Wang, *ACS Nano* **2019**, *13*, 14252.

[33] S. Haldar, K. Roy, R. Kushwaha, S. Ogale, R. Vaidhyanathan, *Adv. Energy Mater.* **2019**, *9*, 1902428.

[34] J. Li, X. Jing, Q. Li, S. Li, X. Gao, X. Feng, B. Wang, *Chem. Soc. Rev.* **2020**, *49*, 3565.

[35] F. Xu, S. Jin, H. Zhong, D. Wu, X. Yang, X. Chen, H. Wei, R. Fu, D. Jiang, *Sci. Rep.* **2015**, *5*, 8225.

[36] Y. Zhu, X. Chen, Y. Cao, W. Peng, Y. Li, G. Zhang, F. Zhang, X. Fan, *Chem. Commun.* **2019**, *55*, 1434.

[37] X. Zhu, S. An, Y. Liu, J. Hu, H. Liu, C. Tian, S. Dai, X. Yang, H. Wang, C. W. Abney, S. Dai, *AIChE J.* **2017**, *63*, 3470.

[38] X. Chen, Q. Dang, R. Sa, L. Li, L. Li, J. Bi, Z. Zhang, J. Long, Y. Yu, Z. Zou, *Chem. Sci.* **2020**, *11*, 6915.

[39] J. Maschita, T. Banerjee, G. Savasci, F. Haase, C. Ochsenfeld, B. V. Lotsch, *Angew. Chem., Int. Ed.* **2020**, *59*, 15750.

[40] J. Park, C. W. Lee, J. H. Park, S. H. Joo, S. K. Kwak, S. Ahn, S. J. Kang, *Adv. Sci.* **2018**, *5*, 1801365.

[41] J. Lee, H. Kim, M. J. Park, *Chem. Mater.* **2016**, *28*, 2408.

[42] C. Peng, G.-H. Ning, J. Su, G. Zhong, W. Tang, B. Tian, C. Su, D. Yu, L. Zu, J. Yang, M.-F. Ng, Y.-S. Hu, Y. Yang, M. Armand, K. P. Loh, *Nat. Energy* **2017**, *2*, 17074.

[43] C. Luo, G.-L. Xu, X. Ji, S. Hou, L. Chen, F. Wang, J. Jiang, Z. Chen, Y. Ren, K. Amine, C. Wang, *Angew. Chem., Int. Ed.* **2018**, *57*, 2879.

[44] T. Yang, Y. G. Liu, D. X. Yang, B. B. Deng, Z. H. Huang, C. D. Ling, H. Liu, G. X. Wang, Z. P. Guo, R. K. Zheng, *Energy Storage Mater.* **2019**, *17*, 374.

[45] S. Xu, G. Wang, B. P. Biswal, M. Addicoat, S. Paasch, W. Sheng, X. Zhuang, E. Brunner, T. Heine, R. Berger, X. Feng, *Angew. Chem., Int. Ed.* **2019**, *58*, 849.

[46] M. Wu, Y. Zhao, B. Sun, Z. Sun, C. Li, Y. Han, L. Xu, Z. Ge, Y. Ren, M. Zhang, Q. Zhang, Y. Lu, W. Wang, Y. Ma, Y. Chen, *Nano Energy* **2020**, *70*, 104498.